

## Effect of post weld artificial aging on the local and global mechanical properties of friction stir welds of aluminum alloy 6061-T6

M.A.Abd Elrahman<sup>a</sup>, M.E.Abd El-Azim<sup>a</sup>, Omyma.H.Ibrahim<sup>a</sup>, M.R.El-koussy<sup>b</sup>

<sup>a</sup>Metallurgy Department, Nuclear Research Center, Atomic Energy Authority, Cairo, Egypt

<sup>b</sup>Metallurgy Department, Faculty of Engineering, Cairo University, Giza, Egypt

### Abstract

The aim of this work is to study the responses to post weld artificial aging (PWAA) of friction stir welds of aluminum alloy 6061-T6 welded at low traverse speed of 125 mm/min and at high traverse speed of 710 mm/min. During welding of either the low traverse speed or high traverse speed weld, the transverse profile of peak temperatures and the local thermal cycles at various distances from the weld center were measured. The transverse hardness profile of the low traverse speed and high traverse speed weld were measured one day after welding and after PWAA. Both immediately after welding and after PWAA the transverse profiles of tensile properties, and strain hardening parameters were determined. Special attention was given to the local properties within the weld weakest region, which greatly affect the overall strength and ductility of the welded joints. The results show that PWAA greatly improve the tensile properties of the high traverse speed weld. For the low traverse speed weld, while PWAA slightly improves yield and ultimate tensile strength, it deteriorates the uniform elongation due to the severe mismatch in local mechanical properties between the various zones of the weld.

### Introduction

Friction stir welding (FSW) is a solid state welding process by which the defects accompanied with fusion welding of aluminum alloys such as voids and cracks can be avoided [1, 2]. FSW also offers several other advantages such as excellent weld metallurgical properties, reduced consumed energy, and absence of shielding gas or flux [1]. In FSW process a rotating tool (consisting of a shoulder and a pin) is inserted into the joint line until the shoulder intimately contacts the upper surface of the workpieces to be welded. By moving the inserted rotating tool forward along the joint line, a joint is created due to friction heating and extensive deformation of the material around the tool [3]. The weld is asymmetric around its center since on one side of the weld (the advancing side) the rotation of the tool is in the same direction of the advancing velocity, while on the other side (the retreating side) the tool rotation is in the opposite direction to the tool advance [4].

AA 6061 is one of the Al-Mg-Si alloys which contains balanced amount of Mg and Si in excess of 1.4% and contains also 0.25% Cu [5]. The commonly assumed precipitation sequence in Al-Mg-Si-Cu

alloys is as follow [6, 7, 8]: super saturated solid solution (SSSS)  $\rightarrow$  Mg and Si co-clusters  $\rightarrow$  GP zones  $\rightarrow$   $\beta''$   $\rightarrow$   $\beta' + Q'$   $\rightarrow$   $\beta$  (Mg<sub>2</sub>Si) + Q. The Mg and Si co-clusters observed at low temperature aging (up to 120 OC) or room temperature natural aging [6, 9, 7]. The GP zones observed at early stages of aging [6] as a fully coherent spherical precipitate [10, 11, 7]. The needle shaped fully coherent precipitate  $\beta''$  is the main strengthening precipitate in the 6xxx aluminum alloys and is responsible for the peak aged condition when its size is optimum [8, 12, 13, 14]. The rod shaped semi-coherent precipitate  $\beta'$  is formed during aging for approximately 80 h at 177 OC [7] or at high temperature aging (24 h at 200 OC) [6].  $\beta'$  formation is responsible for the overaged condition and is accompanied with loss in hardness and strength values from their maximum peak aged values [6, 11]. The lath shaped precipitate Q' is observed during overaging accompanied with  $\beta'$  [6].

The behaviors of the existing precipitates within the 6xxx aluminum alloys during FSW are greatly influenced by the experienced thermal cycles at various zones within the weld [4, 15]. The literature provides some information about the temperature ranges of precipitation and dissolution peaks of the precipitates that may exist within the 6xxx aluminum

alloys during continuous heating. During continuous heating of the supersaturated solid solution alloy, the  $\beta''$  precipitation peak observed at 250 OC [6]. The  $\beta'$  precipitates can be formed directly by coarsening of the existing  $\beta''$  without observed  $\beta''$  dissolution peak [4], then the precipitation peak of  $\beta'$  obtained above 290:320 OC [6, 12, 4] followed by dissolution peak of  $\beta'$  at 350:420 OC [4]. During continuous heating of the peak aged alloy,  $\beta''$  precipitates dissolution observed at  $\sim 260$ OC, then  $\beta'$  precipitates are precipitated at  $\sim 310$ OC, followed by  $\beta'$  dissolution between 350 and 420 OC [4]. Sato and his coworkers [15, 16] studied the effect of peak temperatures experienced by the various zones within the AA 6063-T5 FSW joints on their precipitates structure. They reported that no change in precipitates structure observed below 201 OC and the existing  $\beta''$  precipitates dissolution starts at 250 OC. a high density of  $\beta'$  observed when the peak temperature approaches 302 OC. the  $\beta'$  dissolution temperature lie between 353 and 402 OC. all the existing precipitates dissolve completely at peak temperature of 402 OC. They suggested that all the existing precipitates may dissolve temporarily by rapid thermal cycles during FSW.

The local variations in precipitates structure during FSW greatly affect the strain hardening behavior of the various weld zones [4, 17]. The variation of the strain hardening parameters (dislocation storage rate parameter  $\theta$ , dynamic recovery rate parameter  $\beta$ ) with the change of precipitates structure during the various stages of artificial aging were studied for several 6xxx series aluminum alloy [2, 18, 19]. Their values depend on the content of dissolved solute atoms and on the nature and size of the existing precipitates. The SSSS alloy has higher value of  $\theta$  than the peak aged alloy due to the presence of large amount dissolved solute atoms which cause dynamic precipitation during forming of the SSSS alloy [2, 17, 20]. While the value of  $\theta$  decreases with decreasing the content of solute atoms during aging of the SSSS alloy until a minimum value is obtained at peak aging due to the reduced amount of dynamic precipitation [17], the  $\beta$  value undergoes no significant change [2, 17, 21]. In the peak aged condition, where all the existing solute atoms precipitate as shearable coherent precipitates, both  $\theta$  and  $\beta$  values are at their minimum values. During overaging, as the precipitates size exceeds the shearing/bypassing size, the values of both  $\theta$  and  $\beta$  increases with size until a maximum value are obtained when the precipitates completely loss its coherency with the matrix. Little work studied the local variation of strain hardening parameters of the 6xxx series FSW joints especially of the AA 6061. There is a lack in the information about the strain hardening parameters of the various zones within the FSW joints especially in the immediately after welding and after PWAA conditions.

The differences in structural changes during FSW within different weld zones results in high degree of inhomogeneity in the transverse profiles of hardness, tensile properties, strain hardening parameters

which results in localization of deformation in the weakest region and deteriorate the mechanical properties of the FSW joints [2,4, 17]. Although post weld solution heat treatment and aging is effective in improving the mechanical properties and obtaining homogenous hardness profile of the FSW joints of some of the 6xxx series aluminum alloys [16, 22, 23], it is not suitable for many aluminum alloys applications and also it consumes high amount of energy and cost. So, it is required to study the ability of PWAA, the lower cost, energy saving and more suitable for large and complicated structures, to avoid or at least minimize the mismatch Within the hardness, tensile properties and strain hardening parameters profiles and obtain better combination of mechanical properties at various traverse speeds.

## Experimental Work

FSW of 5 mm thickness AA 6061-T6 plates were carried out using a tungsten carbide FSW tool at rotation rate of 1800 rpm and traverse speeds of 125 and 710 mm/min. the FSW tool has a concave shoulder of 15 mm diameter and a 15° tapered cone pin with 5mm base diameter and 4.3 mm pin length. All the joints welded at 3° tilt angle and 0.15 mm sink depth. During welding, local thermal histories were provided by inserting k-type thermocouples just below tool pin at the weld center and at mid thickness of various distances selected based on the hardness profile of the welds. The macrostructure and microstructure on the transverse cross section was studied by optical microscopy (OM) after etching using keller reagent.

The global tensile properties of the welds were determined by performing tensile tests in the transverse direction (perpendicular to the welding direction) of all the welded joints. For the FSW joints welded at 125 mm/min (which will be called the low traverse speed weld) and at 710 mm/min (which will be called the high traverse speed weld), the local tensile properties and strain hardening parameters of various zones were determined by extracting longitudinal micro-tensile specimens (parallel to the welding direction) from various zones selected based on the micro-hardness profile. For either the transverse and micro longitudinal tensile tests, the tests were carried out immediately after welding (IAW) (within 4 h after welding) and also after PWAA (aging at 160 °C for 18 h).

The strain hardening parameters (the dislocation storage rate  $\theta$  and the dynamic recovery rate  $\beta$ ) which are known as Kock-Mecking-Estrin parameters were extensively used to describe the strain hardening of several 6xxx series aluminum alloys [2, 17, 4, 18, 19]. They can be concluded from the true stress strain curves based on the Voce equation which relates the work hardening rate ( $d\sigma_f/d\varepsilon_p$ ) to  $\theta$ ,  $\beta$  and the increase of flow stress ( $\sigma_f - \sigma_y$ ) [4, 17]:

$$d\sigma_f/d\varepsilon_p = \theta - \beta (\sigma_f - \sigma_y),$$

Where  $\varepsilon_p$  is the plastic strain,  $\sigma_f$  and  $\sigma_y$  are the true flow stress and true yield stress respectively.

For the low traverse speed and high traverse speed welds, Vickers micro-hardness measurements were measured at mid thickness on the transverse cross section using a Vickers indenter with 300 gram load for 10 s. The micro-hardness profiles were measured 1 day after welding (DAW) and after PWAA.

Within the transverse cross section of the joints or the transverse profiles of various mechanical properties, the retreating side is to the right side (the positive sign distances from the weld center) and the advancing side is to the left side (the negative sign distances from the weld center).

## Results

The transverse cross section of the low traverse speed and high traverse speed welds are shown in Figure 1.a and b respectively. Various zones can be distinguished based on the variations in grain structure. Around the weld center, the nugget zone (NZ) has a fine equiaxed recrystallized grain structure as shown in Figure 2c and d. The NZ within either the low traverse speed or high traverse speed weld has a much finer grain structure than the base metal Figure 2a, b and c. The high traverse speed weld NZ has finer grains than the low traverse speed weld NZ. On either side of the NZ, there is a recovered grain structure zone known as the thermomechanically affected zone (TMAZ). The unchanged grain structure regions, that lie outside the TMAZ and that characterized by loss of hardness and yield strength as shown later, are known as heat affected zone (HAZ).



**Figure 1** The macrostructure of the (a) low traverse speed weld (b) high traverse speed weld.

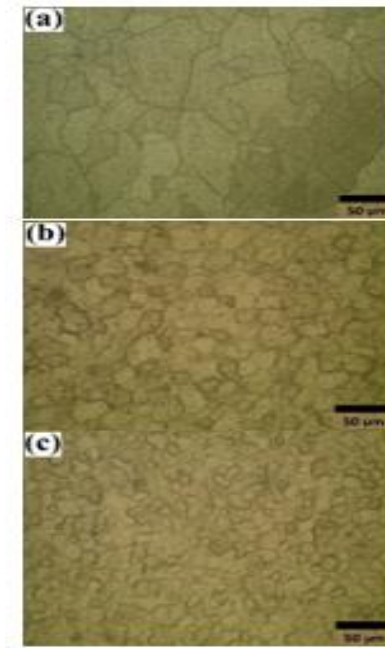


**Figure 2** The grain structure of the (a) base metal (b) low traverse speed weld NZ (c) high traverse speed weld NZ.

The yield strength (YS), ultimate tensile strength (UTS) and uniform elongation (UE) of the low traverse speed and high traverse speed welds both IAW and after PWAA are shown in Figure 3. In the IAW condition, the values of either YS, UTS or UE of the high traverse speed weld is higher than the low traverse speed weld. The YS, UTS and UE values of the welds lie respectively at approximately 40, 60 and 40 % of the base metal values. After PWAA, the UTS, YS values of both welds were improved and the degree of improvement is higher in the high traverse speed weld. While the values of UTS and YS of the low traverse speed weld are slightly improved by PWAA and their values are much lower than that of the base metal, the UE value is greatly deteriorated by PWAA. On the other hand, the UTS, YS and UE values of the high traverse speed weld are improved by PWAA. For the high traverse speed weld, while the value of UTS attains that of the base metal ( $320 \pm 10$ ) and the YS values approaches the base metal value ( $271 \pm 4$ ), the values of UE lie at approximately 71 % of that of the base metal ( $14.1 \pm 0.4$ ). For both welds whether IAW or after PWAA, plastic strain localization occurs within the HAZ especially on the retreating side of the HAZ where fracture always occurs.

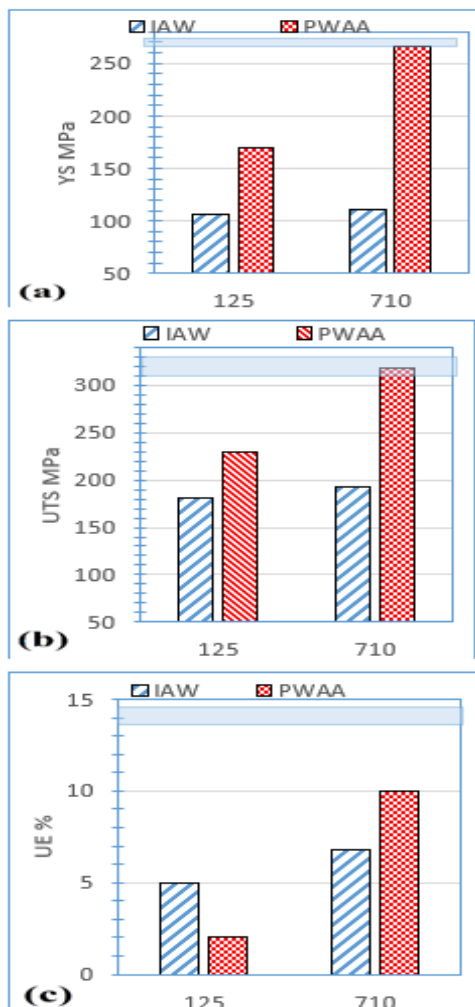


**Figure 3** The tensile properties for the low traverse speed and high traverse speed FSW welded joints both IAW and after PWAA (a) YS, (b) UTS and (c) UE. The colored areas represent the range of parent metal values for each property.

The mid thickness hardness profile across the transverse section of the FSW joints both one day after welding (DAW) and after PWAA for the low traverse speed and high traverse speed weld are shown in Figure 4 a and b respectively. In the DAW condition, both the low traverse speed and high traverse speed welds have a softened region (SOF) around the weld center extending over a distance larger than the mid thickness width of the NZ. Although the SOF region hardness values within the high traverse speed weld is slightly higher than the low traverse speed weld, their values are not greatly differ from the solution treated alloy tested after 1 day at room temperature (58 HV). On either side of the SOF region, there is a minimum hardness region at which the same base metal grain structure is retained. So, it is considered as a minimum hardness heat affected zone (MIN HAZ). The hardness increases with the distance away from the weld center from the MIN HAZ through an intermediate hardness heat affected zone (INT HAZ) until it reaches to a value equal to the base metal hardness ( $122 \pm 2$  HV) at the unaffected base metal zone (BM). Although the hardness profiles for both the high

traverse speed and low traverse speed welds are similar, the width of the overall affected zone is wider in the low traverse speed weld ( $\sim \pm 25$  mm) than the high traverse speed weld ( $\sim \pm 15$  mm). While the MIN HAZ of the low traverse speed weld lie at approximately 8 mm from the weld center, it lie at only 6.5 mm from the weld center in the high traverse speed weld.

The hardness values of all the zones within either low traverse speed or high traverse speed weld increased by PWAA. The degrees of hardness recovery of the various zones within the low traverse speed weld are lower than the high traverse speed weld especially in the MIN HAZ. Although PWAA leads to a significant hardness recovery within the SOF region of either the low traverse speed or high traverse speed weld, the hardness values are not fully recovered. While PWAA leads to a significant hardness recovery in the MIN HAZ of the high traverse speed weld, a limited hardness recovery is obtained in the MIN HAZ of the low traverse speed weld especially on the retreating side. In the BM region there is no change in the hardness value after PWAA.

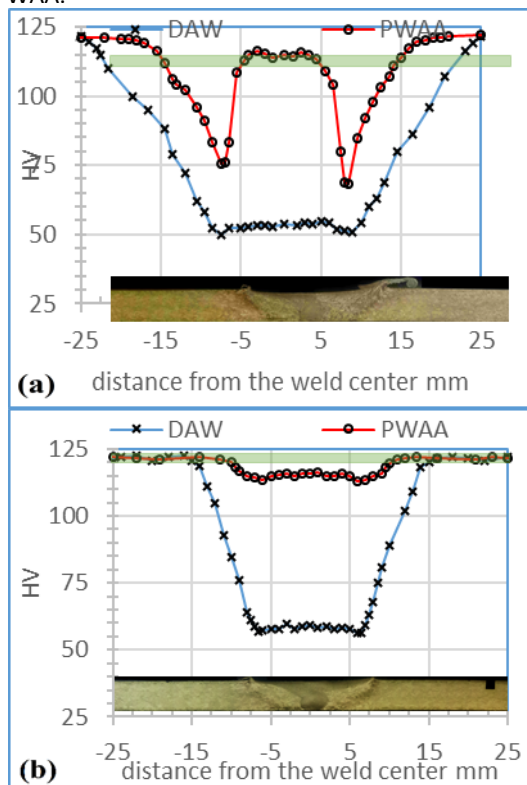


**Figure 4** The mid thickness hardness profile along the transverse cross section in either the DAW and after PWAA conditions of (a) low traverse speed weld (b) high traverse speed weld. The colored areas represent the range of parent metal hardness.

At the same distance from the weld center, the peak temperature is higher in the low traverse speed weld than in the high traverse speed weld as shown in Figure 5 (a). The width of the region experienced peak temperatures higher than  $200^\circ\text{C}$  is larger in the low traverse speed weld than in the high traverse speed weld. The thermal cycles experienced at the NZ and MIN HAZ within both the low traverse speed and high traverse speed welds are shown in Figure 5

(b). The NZ peak temperatures in the low traverse speed weld and high traverse speed weld are 433 and 388 °C respectively. During cooling, the times spent by the NZ within the  $\beta'$  precipitation temperature range, temperatures below the  $\beta'$  start dissolution temperature 350 °C down to the  $\beta'$  start precipitation temperature 290 °C [4], are ~ 6 and 2 seconds for the low traverse speed and high traverse speed weld respectively. Within the MIN HAZ thermal cycle, the MIN HAZ experienced peak temperatures of 353 and 322 °C for the low traverse speed and high traverse speed weld respectively. The times spent within the  $\beta'$  precipitation temperature range are ~ 20 and 4 seconds for low traverse speed and high traverse speed weld respectively.

For either the low traverse speed and high traverse speed weld, the peak temperatures within the INT HAZ lie between the MIN HAZ peak temperatures and 200 °C (below which no significant change in existing precipitates structure or hardness can be detected [9, 15]). The INT HAZ regions that exhibit peak temperatures within the  $\beta'$  precipitation temperature range extend from the MIN HAZ to approximately 14 and 8 mm away from the weld center for the low traverse speed and high traverse speed weld respectively. The INT HAZ regions where the peak temperatures lie below  $\beta'$  precipitation temperature range down to 200 °C extend to ~ 25 and 15 mm away from the weld center for the low traverse speed and high traverse speed weld respectively. Within the INT HAZ regions, the times spent during the local thermal cycles are longer in the low traverse speed weld than the high traverse speed weld.

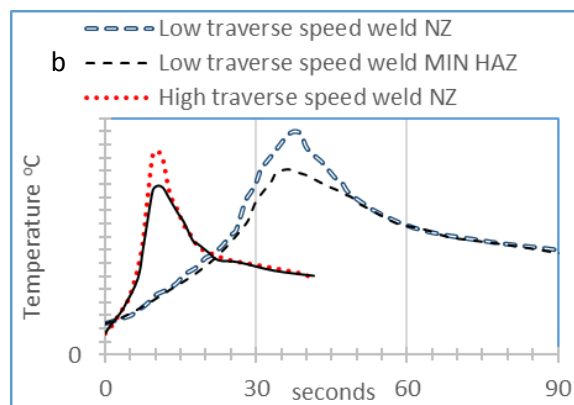
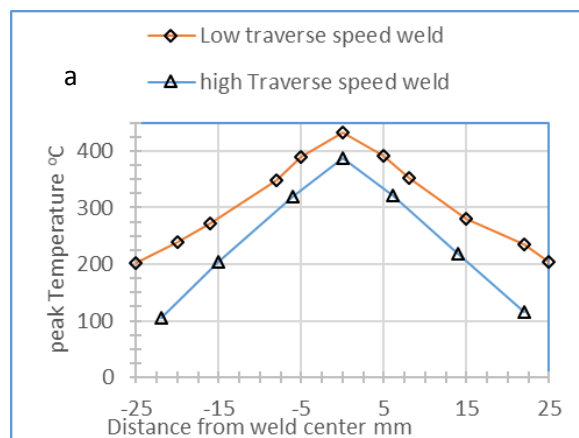


**Figure 5** (a) the peak temperatures transverse profiles during FSW of the low traverse speed and high traverse speed weld (b) the thermal cycles at the weld center and MIN HAZ of the low traverse speed and high traverse speed welds.

The local tensile properties and strain hardening parameters profiles across the transverse section of the low traverse speed and high traverse speed weld are shown in Figure 6. In the IAW condition for either the low traverse speed or high traverse speed weld, The YS profiles (Figure 6a and b) are similar to the hardness profiles (Figure 4a and b). The YS values of the NZ are slightly higher than the MIN HAZ where the YS has a minimum value. The YS values increase from a minimum value with the distance away from the weld center through the INT HAZ until they attain the BM value. The UTS profiles are similar to the YS profiles, but the UTS values of the NZs are much higher than the MIN HAZ where the UTS has a minimum value. The UE values of the NZ are much higher than the BM and approach the value of the solution treated alloy. The UE values of the high traverse speed weld MIN HAZ are also higher than the BM, but the low traverse speed weld MIN HAZs have a much lower UE than the BM. The strain hardening parameters  $\theta$  and  $\beta$  have a minimum value in the BM. In both the low traverse speed and high traverse speed weld, while the NZs have a value of  $\theta$  higher than the BM, there are no significant difference in the values of  $\beta$  with that of the BM. While the low traverse speed weld MIN HAZs have a significant high value of both  $\theta$  and  $\beta$ , the high traverse speed weld MIN HAZs have a value slightly higher than the BM.

In both the low traverse speed and high traverse speed welds, PWAA increase the values of either UTS or YS in all the softened zones. While the YS and UTS values of the high traverse speed weld MIN HAZ are significantly improved by PWAA, their values improvement in the low traverse speed weld MIN HAZ by PWAA is limited especially in the retreating side. The UE values of the MIN HAZ is lowered by PWAA especially in the low traverse speed weld. The  $\theta$  and  $\beta$  values of the low traverse speed weld MIN HAZ increases by PWAA. While PWAA slightly decrease the  $\theta$  value within the high traverse speed weld NZ and MIN HAZ, it slightly raise the values of  $\beta$ .

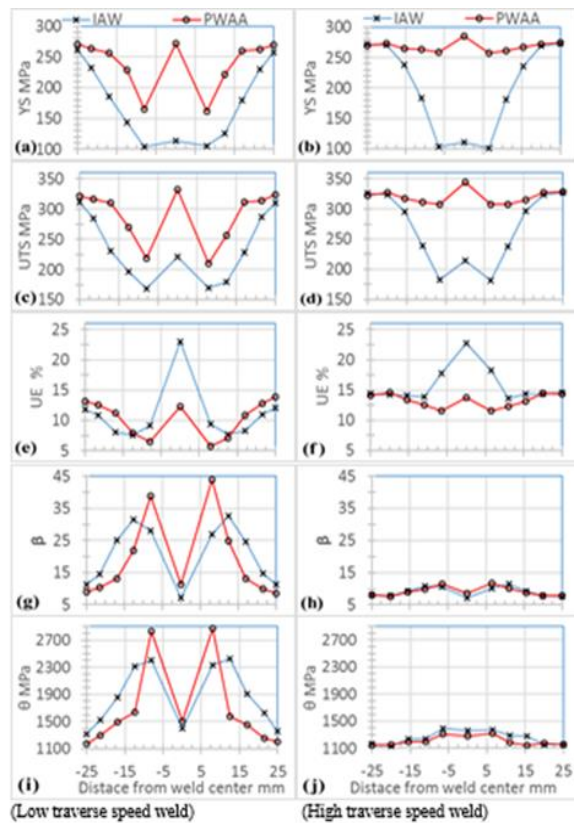


**Figure 6** The local tensile properties profiles across the transverse section for the low traverse speed and high traverse speed welds (a, b) YS, (c, d) UTS, (e, f) UE, (g, h)  $\beta$  and (i, j)  $\theta$ .

## Discussion

### Softening during FSW and hardness recovery by PWAA

In general, the global and local mechanical properties of the FSW joints greatly depend on the precipitate structural variation during the welding process. During FSW of the peak aged 6xxx series aluminum alloys, the existing  $\theta''$  precipitates may be survived, dissolved, coarsened or transformed to the less strengthening semi-coherent  $\theta'$  particles depending on the local thermal cycle experienced by each zone [4, 15]. In the IAW condition, the drop in hardness within the welded joints softened regions, as shown in Fig. 4a and b, may be due to dissolution and/or coarsening of the existing  $\theta''$  precipitates or precipitation of  $\theta'$ . Within all the softened zones of either the low traverse speed or high traverse speed welds, the hardness recovery by PWAA indicates that a portion of the existing  $\theta''$  precipitates dissolved during FSW resulting in saturation with solute atoms. The higher the degree of hardness recovery by PWAA means the higher the degree of dissolution. The loss in the ability to restore the peak aged hardness value by PWAA within the softened regions indicates that during FSW a part of the existing  $\theta''$  precipitates may be coarsened and/or transformed to  $\theta'$  or the solute atoms resulting from dissolution of the existing precipitates may be consumed by precipitation of  $\theta'$ .

During welding of equal distances, the time spent and the number of tool rotations during the low traverse speed weld (125 mm/min) are 5.6 times greater than that during the high traverse speed

weld (710 mm/min). So, the low traverse speed weld has higher amount frictional heating due to the higher rotations per unit length than the cold weld. Hence, for the same location within the weld, the peak temperature value and also the time spent above any specified temperature is higher in the low traverse speed weld than the high traverse speed weld as shown in Fig. 5a and b.

Within the NZ of either the low traverse speed or high traverse speed weld, the high degree of hardness recovery by PWAA indicates the presence of a large amount of solute atoms resulting from the dissolution of the existing  $\theta''$  during FSW. During FSW, The low traverse speed weld NZ experienced peak temperature of 433 °C which is higher than the solvus temperature of  $\theta'$  (lie between 350 and 402 °C [15]). So, this peak temperature is sufficient to dissolve temporarily all the existing precipitates as reported by Sato and his coworkers [15] in their study of AA6063 FSW. During cooling from the low traverse speed weld NZ peak temperature, the time spent within the  $\theta'$  precipitation temperature range, approximately between 290 and 350 °C [4], is ~ 6 seconds and some  $\theta'$  may be formed. The peak temperature experienced by the high traverse speed weld NZ (388 °C) is also sufficient to obtain high degree of hardness recovery during PWAA or in other words high degree of precipitates dissolution and supersaturation with solute atoms. The time spent by the cold weld NZ within the  $\theta'$  precipitation temperature range is ~ 2 seconds. After PWAA of either the low traverse speed or high traverse speed weld, the slightly lower NZ hardness value than the BM peak hardness value suggests the formation of little amount of  $\theta'$  during cooling. In the IAW condition for both welds, the high degree of supersaturation within the NZ is consistent with the relatively high value of dislocation storage rate parameter  $\theta$  and the low value of dynamic recovery rate  $\beta$  which are similar to the strain hardening parameters of the solution treated alloy.

It is obtained from the MIN HAZ thermal cycles that the low traverse speed weld MIN HAZ peak temperature 353 °C is higher than the high traverse speed weld MIN HAZ peak temperature 322 °C and the time spent within the  $\theta'$  precipitation temperature range are ~ 20 and 4 seconds for the low traverse speed and high traverse speed welds respectively. This suggests that  $\theta'$  may precipitates within the MIN HAZ especially in the low traverse speed weld. The limited hardness recovery within the MIN HAZ during PWAA of the low traverse speed weld indicates that a large amount of the solute atoms is consumed by the precipitation of a less strengthening  $\theta'$  precipitates during FSW. This is consistent with the high values of  $\theta$  and  $\beta$  within the IAW low traverse speed weld MIN HAZ (Figure 6 g and i). So, it is suggested that the IAW structure of low traverse speed weld MIN HAZ consists of a limited degree of solute atoms supersaturation accompanied with a relatively large amount of  $\theta'$  precipitates. On the other hand, the high traverse speed weld MIN HAZ has a high hardness recovery

during PWAA which is slightly lower than that of the high traverse speed weld NZ at which the hardness value after PWAA approaches that of the BM. This suggests that the structure of high traverse speed weld MIN HAZ consists of a large degree of solute atoms supersaturation accompanied with some  $\theta'$  precipitates slightly greater than that exist in the high traverse speed weld NZ. This is consistent with the slightly higher value of  $\beta$ , in the IAW condition, of the high traverse speed weld MIN HAZ than the NZ and relatively high values of  $\theta$  as that of the NZ (Fig. 6h and j). Within the high traverse speed weld MIN HAZ, PWAA decreases the value of  $\theta$  which is consistent with the reduction of dissolved solute atoms, which is accompanied with reduction in dynamic precipitation [17], by precipitation of  $\theta''$ .

Within the low traverse speed weld INT HAZ regions that exhibit peak temperatures lie within the  $\theta'$  precipitation temperature range, although the obtained hardness recovery by PWAA is better than in the MIN HAZ, it is still very limited because  $\theta'$  particles may precipitate during the time spent within the  $\theta'$  precipitation temperature range resulting in low amount of supersaturated solute atoms. The decrease in peak temperature with the distance away from the weld center may be accompanied with reduced amount of  $\theta'$  precipitation and increased degree of supersaturation with solute atoms. So, the degree of hardness recovery by PWAA increased with the distance away from the weld center. This is consistent with the high values of  $\theta$  and  $\beta$ , in either the IAW or after PWAA conditions, within the low traverse speed weld INT HAZ region adjacent to the MIN HAZ and the decrease of their values with the distance away from the weld center (Figure 6g and i). On the other hand, within the high traverse speed weld INT HAZ regions that exhibit peak temperatures lie within the  $\theta'$  precipitation temperature range, the hardness recovery by PWAA is slightly higher than the high traverse speed weld MIN HAZ which has relatively high hardness recovery. The short time spent at the relatively low peak temperatures, within the  $\theta'$  precipitation temperature range, exhibited by those regions suggests the formation of very small amount of  $\theta'$  precipitates and the presence of large degree of supersaturation. Again the hardness recovery by PWAA increases with the distance away from the weld center because the reduced amount of  $\theta'$  precipitates and increased degree of solute atoms supersaturation. This is consistent with the slightly higher values of  $\theta$  and  $\beta$ , in either the IAW or after PWAA conditions, within the high traverse speed weld INT HAZ region adjacent to the MIN HAZ and the decrease of their values with the distance away from the weld center (Figure 6h and j).

For either the low traverse speed or high traverse speed weld, within the INT HAZ that exhibit peak temperatures below the  $\theta'$  precipitation temperature but higher than 200 °C, above which the stability of  $\theta''$  precipitates is reduced [9, 15, 16], some of the existing  $\theta''$  precipitates may be dissolved, coarsened or remained. Within this region, the decrease in peak

temperature with the distance away from the weld center may result in decreased amount of  $\theta''$  coarsening and increased amount of  $\theta''$  dissolution. So, the degree of hardness recovery increased with the distance away from the weld center until the hardness values are fully recovered for both the low traverse speed and high traverse speed welds.

### Local and global tensile properties

For both the low traverse speed and high traverse speed weld in either the IAW condition or after PWAA, there are no significant differences between the YS and UTS values of the welded joint and their local values in the MIN HAZ of the same joint as can be observed from Figure 3a and b and Figure 6a, b, c and d. Hence, the YS and UTS of the welded joint are controlled by their values in the MIN HAZ which is the weakest zone within the weld.

In the IAW condition for either the low traverse speed or high traverse speed weld, although the YS values of the NZ and the MIN HAZ are not significantly different, the existence of larger amount of  $\theta'$  precipitates within the MIN HAZ than in the NZ especially in the low traverse speed weld results in lower strain hardening capacity in the MIN HAZ, as evidenced by a high recovery rate  $\beta$  (Figure 6g and h). So, the UTS of the MIN HAZ is lower than the NZ in either the low traverse speed or high traverse speed weld (Fig. 6c and d). During tensile tests of either the low traverse speed or high traverse speed welded joints, the lower strain hardening capacity (higher  $\beta$ ) and slightly lower YS of the MIN HAZ than the NZ implies that the rate of strain hardening within the NZ is larger than the MIN HAZ. So, with increasing the tensile strain the MIN HAZ becomes weaker than the NZ and other surrounding regions resulting in triaxial state of stress within the MIN HAZ and deformation localization within the MIN HAZ. This deformation localization within the MIN HAZ results in further increase in the stress triaxiality. The triaxial state of stress results in void formation and coalescence within the MIN HAZ at which fracture occurs. The higher strain hardening capacity (lower  $\beta$ ) of the high traverse speed weld MIN HAZ than the low traverse speed weld MIN HAZ results in higher UTS value within the high traverse speed weld MIN HAZ. So, the high traverse speed weld has higher UTS than the low traverse speed weld and also has higher UE due to delayed deformation localization to higher stresses.

After PWAA for either the low traverse speed or high traverse speed weld, although the YS and UTS values of all the zones were improved, the variation in the degree of solute atoms supersaturation between various zones affect this degree of improvement. Within the low traverse speed weld MIN HAZ, the existence of relatively large amount of  $\theta'$  precipitates and limited degree of solute atoms supersaturation, as evidenced by the high  $\theta$  and  $\beta$  values and also by the limited hardness recovery by PWAA within this zone, limit the improvement of YS by PWAA. The improvement of the UTS value by PWAA of the low traverse speed weld MIN HAZ is

also limited because of the high value of dynamic recovery rate  $\beta$  and low value of  $Y_S$  after PWAA as shown in Fig.6a, c and g. Hence, the  $Y_S$  and UTS values of the overall low traverse speed welded joint after PWAA are limited to 59% and 65% of the base metal value of  $Y_S$  and UTS respectively as shown in Figure 3 a and b. On the other hand, the limited amount of  $\beta'$  precipitates and high degree of solute atoms supersaturation within the high traverse speed weld MIN HAZ, as evidenced by the high degree of hardness recovery by PWAA, result in high degree of  $Y_S$  and UTS improvement by PWAA. Hence, the  $Y_S$  and UTS values of the overall high traverse speed welded joint are highly improved by PWAA to 94% and 96% of the base metal value of  $Y_S$  and UTS respectively. The significantly higher degree of  $Y_S$  and UTS improvement by PWAA in the high traverse speed weld MIN HAZ than in the low traverse speed weld MIN HAZ demonstrate why the  $Y_S$  and UTS values of the welded joint are further improved by PWAA with increasing the FSW traverse speed as shown in Figure 3 a and b.

The low traverse speed weld MIN HAZ and adjacent portion of the INT HAZ (that experience peak temperatures lie within the  $\beta'$  precipitation temperature range) have limited degree of supersaturation with solute atoms and significantly higher amount  $\beta'$  precipitates than the low traverse speed weld NZ and other INT HAZ regions. So, the improvements of hardness,  $Y_S$ , and UTS by PWAA in the former zones are much limited than in the later zones. This demonstrates the unfavorable high degree of mismatch that observed within the PWAA low traverse speed weld transverse profiles of hardness,  $Y_S$  and UTS as shown in Figure 4 a and Figure 6 a and c respectively. This high degree of mismatch in  $Y_S$ , UTS between the MIN HAZ and other surrounding regions within the PWAA low traverse speed weld results in multiaxial stress condition within the MIN HAZ during deformation of the welded joint. These stresses enhance the initiation and growth of voids at the  $\beta'$ -matrix interface which accelerate the occurrence of failure of the welded joint within the MIN HAZ. This results in lower UE in the PWAA condition than in the IAW condition.

On the other hand, the high traverse speed weld MIN HAZ and INT HAZ (that experience peak temperatures lie within the  $\beta'$  precipitation temperature range) have a degree of supersaturation with solute atoms not significantly lower than the high traverse speed weld NZ and other INT HAZ regions. So, the degree of improvement of hardness,  $Y_S$ , and UTS by PWAA within the former zones are not much lower than the later zones. Hence, a low degree of mismatch is observed within the PWAA high traverse speed weld transverse profiles of hardness,  $Y_S$  and UTS as shown in Figure 4 b and Figure 6 b and d respectively. This low degree of mismatch in the values of  $Y_S$  and UTS values between the MIN HAZ and the surrounding regions results in a large strain over the entire PWAA high traverse speed weld before the deformation is localized within the MIN HAZ. Hence, the UE value of

the high traverse speed joints is improved by PWAA to approximately 71% of the base metal UE value.

## Conclusions

In this study, the tensile properties of FSW of AA 6061-T6 joints welded at 125 mm/min (low traverse speed weld) and 710 mm/min (high traverse speed weld) were studied both immediately after welding and after post weld artificial aging. The transverse profiles of hardness, tensile properties and strain hardening parameters were determined for both welds. The local thermal histories and the transverse peak temperature profiles during welding were also determined for both welds. The results of this study lead to the following conclusions:

- The hardness recovery after PWAA in all the zones within either the low traverse speed or high traverse speed weld implies that some of the existing  $\beta''$  dissolve resulting in some degree of solute atoms supersaturation in all the zones in both welds. The lower degree of hardness recovery by PWAA and the higher values of  $\theta$  and  $\beta$  within the low traverse speed weld MIN HAZ than the high traverse speed weld MIN HAZ may imply that the low traverse speed weld MIN HAZ structure consists of higher density of  $\beta'$  particles with a lower degree of solute atoms supersaturation than the high traverse speed weld MIN HAZ. Hence, the higher the welding traverse speed the higher the ability to recover the hardness by PWAA within the MIN HAZ.
- The strength of the welded joints are controlled by the strength value of the weakest zone within the weld (MIN HAZ). The limited improvement of the low traverse speed weld MIN HAZ strength by PWAA results in  $Y_S$  and UTS values of the low traverse speed welded joints limited to 59 and 65% respectively of the base metal values. On the other hand, the significant improvement in strength of the high traverse speed weld MIN HAZ by PWAA results in  $Y_S$  and UTS values of the high traverse speed welded joints are 94 and 96% respectively of the base metal values. In brief, the ability to improve the welded joint strength by PWAA is higher in high traverse speed welded joints.
- The high degree of mismatch in  $Y_S$  and UTS values of the MIN HAZ and other surrounding regions within the PWAA low traverse speed weld, due to the limited ability of PWAA to improve the  $Y_S$  and UTS within the MIN HAZ, results in severe deformation localization within the MIN HAZ during tension testing of the PWAA low traverse speed welded joint. So, PWAA greatly deteriorates the UE value of the low traverse speed joints.
- The slight degree of mismatch in  $Y_S$  and UTS values of the MIN HAZ and other surrounding regions within the PWAA high traverse speed weld, due to the slight difference in the ability of PWAA to improve the  $Y_S$  and UTS between the MIN HAZ and other surrounding regions, results in slight deformation localization within the MIN HAZ during tension testing of the PWAA low traverse speed welded joint. So, PWAA improves the UE value of the high traverse speed joints.

## References

- [1] **R.S. Mishra, Z.Y. Ma.** Friction stir welding and processing. *Materials Science and Engineering R* 2005; 50:1-78.
- [2] **Simar, Y. Bréchet, B. de Meester, A. Denquin, C. Gallais, T. Pardoën.** Integrated modeling of friction stir welding of 6xxx series Al alloys: Process, microstructure and properties. *Progress in Materials Science* 2012; 57:95-183.
- [3] **Douglas e. Burkes, Neil p. Hallinan, karen I. Shropshire, and Peter b. Wells.** Effects of applied load on 6061-t6 aluminum joined employing a novel friction bonding process. *Metallurgical and materials transactions A* 2008; 39: 2852-61.
- [4] **A. Simar, Y. Bréchet, B. de Meester, A. Denquin, T. Pardoën.** Microstructure, local and global mechanical properties of friction stir welds in aluminium alloy 6005A-T6. *Materials Science and Engineering A* 2008; 486:85-95.
- [5] **J. Polmer, Light alloys,** E. Arnold, Hodder and Stoughton Ltd. UK, second edition, (1989).
- [6] **Murshid Imam, Vikranth Racherla, Kajal Biswas.** Effect of post-weld natural aging on mechanical and microstructural properties of friction stir welded 6063-T4 aluminium alloy. *Materials and Design* 2014; 6: 675-86.
- [7] **J. Buha, R.N. Lumley, A.G. Crosky, K. Hono.** Secondary precipitation in an Al-Mg-Si-Cu alloy. *Acta Materialia* 2007; 55: 3015-24.
- [8] **D.J. Chakrabarti, David E. Laughlin.** Phase relations and precipitation in Al-Mg-Si alloys with Cu additions. *Progress in Materials Science* 2004; 49: 389-410.
- [9] **M. Murayama and k. Hono.** Pre-precipitate clusters and precipitation processes in al-mg-si alloys. *Acta metallurgica* 1999; 47: 1537-48.
- [10] **S. J. Andersen, H. W. Zandbergen, J. Jansen, C. Traholt, U. Tundal and O. Reiso.** The crystal structure of the  $\beta''$  phase in Al-Mg-Si alloys. *Acta metallurgica* 1998; 46: 3283-98.
- [11] **R. Vissers, M.A. van Huis, J. Jansen, H.W. Zandbergen, C.D. Marioara, S.J. Andersen.** The crystal structure of the  $\beta'$  phase in Al-Mg-Si alloys. *Acta Materialia* 2007; 55:3815-23.
- [12] **A. Gaber, M.A. Gaffar, M.S. Mostafa, E.F. Abo Zeid.** Precipitation kinetics of Al-1.12 Mg<sub>2</sub>Si-0.35 Si and Al-1.07 Mg<sub>2</sub>Si-0.33 Cu alloys. *Journal of Alloys and Compounds* 2007; 429:167-75.
- [13] **S. Tsao, C. Y. Chen, U. S. Jeng, T. Y. Kuo.** Precipitation kinetics and transformation of metastable phases in Al-Mg-Si alloys. *Acta Materialia* 2006; 54: 4621-31.
- [14] **W.F. Miao and D.E. Laughlin.** Precipitation hardening in aluminum alloy 6022. *Scripta Materialia* 1999; 40: 873-78.
- [15] **Yutaka S. Sato, Hiroyuki Kokawa, Masatoshi Enomoto, and Shigetoshi Jogan.** Microstructural Evolution of 6063 Aluminum during Friction Stir Welding. *Metallurgical and materials transactions A* 1999; 30: 2429-37.
- [16] **Yutaka S. Sato, Hiroyuki Kokawa, Masatoshi Enomoto, Shigetoshi Jogan, and Takenori Hashimoto.** Precipitation Sequence in Friction Stir Weld of 6063 Aluminum during Aging. *Metallurgical and materials transactions A* 1999;30: 3125-30.
- [17] **A. Simar, Y. Brechet, B. de Meester, A. Denquin, T. Pardoën.** Sequential modeling of local precipitation, strength and strain hardening in friction stir welds of an aluminum alloy 6005A-T6. *Acta Materialia* 2007; 55: 6133-43.
- [18] **S. Esmaili, L.M. Cheng, A. Deschamps, D.J. Lloyd, W.J. Poole.** The deformation behaviour of AA6111 as a function of temperature and precipitation state. *Materials Science and Engineering A* 2001; 319-321: 461-65.
- [19] **L.M. Cheng, W.J. Poole, J.D. Embury, and D.J. Lloyd.** The Influence of Precipitation on the Work-Hardening Behavior of the Aluminum Alloys AA6111 and AA7030. *Metallurgical and materials transactions A* 2003; 34: 2473-81.
- [20] **A. Deschamps, Y. Brechet, C. J. Necker, S.Saimoto, J. D. Embury.** study of large strain deformation of dilute solid solutions of Al-Cu alloy using channel-die compression. *Materials science and engineering A* 1996; 207: 143-52.
- [21] **G. Fribourg, Y. Brechet, A. Deschamps, A. Simar** Microstructure-based modelling of isotropic and kinematic strain hardening in a precipitation-hardened aluminium alloy. *Acta Materialia* 2011; 59: 3621-3635.
- [22] **K. N. Krishnan.** The effect of post weld heat treatment on the properties of 6061 friction stir welded joints. *Journal of materials science* 2002; 37: 473-80.
- [23] **G. Madhusudhan Reddy, P. Mastanaiah, K. Sata Prasad and T. Mohandas.** Microstructure and mechanical property correlations in AA 6061 aluminium alloy friction stir welds. *Transactions of the Indian Institute of Metals* 2009; 62: 49-58.